


PARAMETRIC STUDY OF A HORIZONTAL AXIS WIND TURBINE WITH SIMILAR CHARACTERISTICS TO THOSE OF THE VILLONACO WIND POWER PLANT

Santiago Sánchez ^{a1,b1}, Victor Hidalgo ^{a2,b2,c*}, Martin Velasco ^{a3,b3}, Diana Puga ^d,
P. Amparo López-Jiménez ^{e1}, Modesto Pérez-Sánchez ^{e2,*} 

^aDepartamento de Ingeniería Mecánica, Escuela Politécnica Nacional, Quito 170525, Ecuador.

^bLaboratorio Informática-Mecánica, Escuela Politécnica Nacional, Quito 170525, Ecuador.

^cCarrera Pedagogía Técnica de la Mecatrónica, Facultad de Filosofía, Letras y Ciencias de la Educación, Universidad Central Del Ecuador.

^dState Key Laboratory of Hydro Science & Engineering, Tsinghua University, Beijing 100084, China.

^eHydraulic and Environmental Engineering Department, Universitat Politècnica de València, 46022 Valencia, Spain.

^{a1} santiago.sanchez01@epn.edu.ec, ^{a2} victor.hidalgo@epn.edu.ec, ^{a3} martin.velasco@epn.edu.ec, ^d dnd20@mails.tsinghua.edu.cn,
^{e1} palopez@upv.es, ^{e2} mopesan1@upv.es

Abstract:

The present paper focuses on the selection of parameters that maximize electrical energy production of a horizontal axis wind turbine using Python programming language. The study takes as reference turbines of Villonaco wind field in Ecuador. For this aim, the Blade Element Momentum (BEM) theory was implemented, to define rotor geometry and power curve. Furthermore, wind speeds were analyzed using the Weibull probability distribution and the most probable speed was 10.50 m/s. The results were compared with mean annual energy production of a Villonaco's wind turbine to validate the model. Turbine height, rated wind speed and rotor radius were the selected parameters to determine the influence in generated energy. Individual increment in rotor radius and rated wind speed cause a significant increase in energy produced. While the increment in turbine's height reduces energy generated by 0.88%.

Keywords: parametric study; wind turbine; Python; Weibull; energy.

Cite as: Sánchez, S., Hidalgo, V., Velasco, M., Puga, D., López-Jiménez, P.A., Pérez-Sánchez, M. (2021). Parametric study of a horizontal axis wind turbine with similar characteristics to those of the Villonaco wind power plant. *J Appl Res Eng Technol & Engineering*, 2(2), 51-62. <https://doi.org/10.4995/jarte.2021.15056>

1. Introduction

Renewable energy sources (e.g., wind, hydropower, geothermic, solar and biofuels) are considered a valuable option to reduce the emission of polluting gases that come from the use of fossil fuels to generate electricity (Rehman et al., 2018). Nowadays, the wind and solar photovoltaic technologies present the greatest cost reduction due to their wide use (Carta González et al., 2009; International Energy Agency, 2019; Ritchie & Roser, 2017).

In 2018, the total generation of electricity from renewable energies was 450 TWh, representing an increase of 7% when it is compared to 2017. Respectively, 90% of this growth corresponds to the use of wind, hydropower and solar photovoltaic technologies (International Energy Agency, 2019).

In the last decade, Ecuador had promote an important impulse to the generation of electricity using renewable energies (Arconel, 2015), focusing on the change of the productive matrix. For this reason, many facilities had been built. As an example, one of them is located in the south region of the country, 14 km away from Loja city at 2720 msl, which is called Villonaco wind power plant (CEV). This wind farm has 11 aerogenerators, which

have a nominal power of 1.5 MW each, having a mean-year production of 59.57 GWh. Nevertheless, between 2014 and 2018 the peak was higher, having a mean-year production of 78.39 Gwh (Corporación Eléctrica del Ecuador, 2016a, 2019b). The surplus of energy produced with respect to the energy estimated indicates a deficient operating condition. To maximize the electricity generation is needed to develop a methodology that allows identifying the parameters that affect the most the operation of the turbines. Therefore, it is necessary to select the appropriate values for the local operating conditions.

Currently, the BEM theory has been used the most to evaluate the performance of wind turbines. This mathematical model is defined by the combination of the Momentum Theory and the Blade Element (Bakırcı & Yılmaz, 2018; Manwell et al., 2009). Manwell et al. (2009) and Letcher (2017) state that the application of BEM theory is enough in the rotor design of the wind turbine. El Khchine & Sriti (2018) and Biadgo & Aynekulu (2017) point out the wide use of this theory in the industry and scientific research because of its allowance of defining the optimal rotor geometry. Also, BEM theory can be applied to build the power curve of the turbine (Lanzafame & Messina, 2010).

*Corresponding author: Victor Hidalgo, victor.hidalgo@epn.edu.ec; Modesto Pérez-Sánchez, mopesan1@upv.es

The analysis of the wind characteristics is fundamental to quantify the energetic resource of the site where the turbine will be located (Gul et al., 2019). The Weibull distribution of two parameters (shape and scale) is the most used to process wind data due to its flexibility and simplicity (Gul et al., 2019). As a result, the probabilistic density function is obtained for the wind velocities registered.

In order to determine the energy produced all over the year, the power curve of the turbine is needed, and the probabilistic distribution of the wind velocities must be considered (Mathew & Philip, 2011; Ministerio de Electricidad y Energía Renovable, 2013).

2. Description of mathematical model

2.1. Wind turbine

The wind turbine is a device that transforms kinetic energy from the wind into electricity, commonly using three blades (Manwell et al., 2009; Renewable Energy World, 2019). Figure 1 shows the energy generated in terms of wind velocity (International Renewable Energy Agency, 2019). This figure contains three important points: (i) Cut-in speed: is the minimum wind velocity at which the turbine starts delivering useful power (Manwell et al., 2009); (ii) Rated wind speed: is the wind velocity at which the rated power (maximum power of the generator) is achieved (Manwell et al., 2009); and (iii) Cut-out speed: is the maximum wind velocity at which the turbine can deliver power (at this condition the turbine is turned off to avoid any damage) (Manwell et al., 2009).

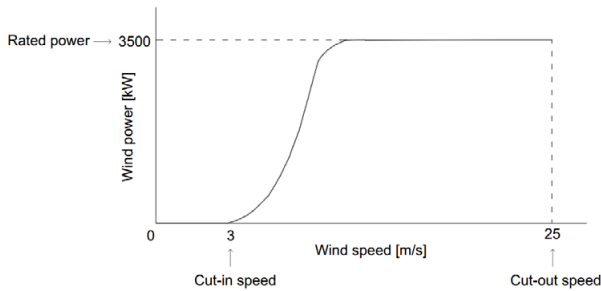


Figure 1: Power curve (International Renewable Energy Agency, 2019).

2.2. Weibull distribution

Weibull distribution is the most convenient function to define the wind regime characteristics because it represents the variation of the wind speed with an acceptable accuracy level (Gul et al., 2019). The probabilistic density function and the Weibull cumulative distribution are defined by Equation (1) - (2), as follows:

$$f(U) = \frac{k}{c} \left(\frac{U}{c}\right)^{k-1} e^{-\left(\frac{U}{c}\right)^k}, \quad (1)$$

$$F(U) = 1 - e^{-\left(\frac{U}{c}\right)^k}, \quad (2)$$

Where U represents wind velocity [m/s], k is the shape factor (dimensionless), and c is the scale factor [m/s]. Based on (Gul et al., 2019; Mathew & Philip, 2011; Topaloğlu & Pehlivan, 2018), these are determined by the following expressions:

$$k = \left(\frac{\sigma}{\bar{x}}\right)^{-1,086}, [-] \quad (3)$$

$$c = \bar{x} * \left(0,568 + \frac{0,433}{k}\right)^{\frac{1}{k}}, [\text{m/s}] \quad (4)$$

where σ is the standard deviation of the wind velocities [m/s], and \bar{x} is the mean wind velocity [m/s].

There are two additional Weibull indicators: The most probable wind velocities U_{mp} , and the velocity which carries the most energy, $U_{máxE}$. Based on (Gul et al., 2019), both are defined as follows:

$$U_{mp} = c * \left(1 - \frac{1}{k}\right)^{\frac{1}{k}}, [\text{m/s}] \quad (5)$$

$$U_{máxE} = c * \left(1 + \frac{2}{k}\right)^{\frac{1}{k}}, [\text{m/s}] \quad (6)$$

In the design of the wind turbine, the nominal velocity must be close to $U_{máxE}$ (Oyedepo et al., 2012). Temperature, direction and velocity of the wind were obtained from the Ecuadorian Electric Corporation (CELEC EP GENSUR), which corresponds to measurements done in time slots of 10 minutes along 24 hours a day in the period between 2015 and 2019. Wind velocity was recorded at 20.8 m, 40.8 m and 62.8 m height and the temperature was measured only at 62 m.

The mean wind velocity obtained between 2015 and 2019 is used to determine the average probabilistic density functions and the Weibull cumulative distribution in these years.

2.3. BEM Theory

BEM theory equals the normal force and the torque equations obtained from momentum theory and Blade element to determine the expressions, which define axial (a) and tangential (a') induction factors (Eq. 7 - 8). These dimensionless factors express the reduction of the wind velocity that goes through the rotor and the ratio between angular velocities of the air and rotor, respectively (Manwell et al., 2009).

$$a = \frac{1}{\left[1 + \frac{4\sin^2\varphi}{s'C_l\cos\varphi}\right]} \quad (7)$$

$$a' = \frac{1}{\left[\frac{4\cos\varphi}{s'C_l} - 1\right]}, \quad (8)$$

Where φ is the relative wind angle [°], s' is the local solidity which is dimensionless, and C_l is the dimensionless lift coefficient.

The theory is focus on an iterative process in which at the beginning is assumed that the axial and tangential induction factors are equal to zero. Then the absolute subtraction control the process until it reaches a tolerance lower than 0.001 (Najafian Ashrafi et al., 2015).

Figure 2 shows the cross section of the Blade and the relationship between angles, velocities and forces (Manwell et al., 2009).

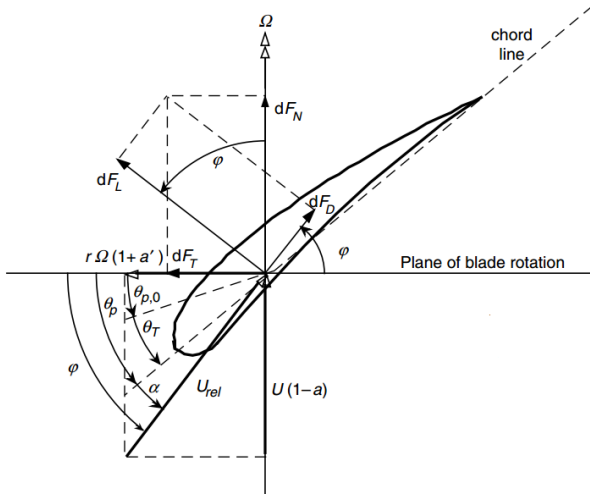


Figure 2: Blade cross section (Manwell et al., 2009).

Equation (9) and Eq.(12-18) are part of the iterative process and they are updated until the aforementioned condition is met (Manwell et al., 2009). The relative wind angle \$\phi\$ can be obtained using the following expression:

$$\phi = \tan^{-1}\left(\frac{U(1-a)}{\Omega r(1+a')}\right) = \tan^{-1}\left(\frac{1-a}{(1+a')\lambda_r}\right), \text{ [}^\circ\text{]} \quad (9)$$

where \$U\$ is wind velocity [m/s], \$a\$ is the axial induction factor, \$a'\$ is the tangential induction factor, \$\Omega\$ is the angular velocity of the rotor [rad/s], \$r\$ is the mean radius of the blade [m], and \$\lambda_r\$ is the local specific velocity. The local specific velocity relates the rotor velocity of a mean radius of the blade and the wind velocity as follows:

$$\lambda_r = \frac{\Omega r}{U} = \frac{\lambda R}{R}, \text{ [-]} \quad (10)$$

where \$\lambda\$ is the specific tip velocity \$\lambda\$ or TSR (tip-speed ratio) and \$R\$ the rotor radius.

The specific tip velocity relate the tip velocity of the blade and the free stream wind velocity as follows:

$$\lambda = \frac{\Omega R}{U}, \text{ [-]} \quad (11)$$

The setting angle \$\theta_p\$ is expressed in the following way

$$\theta_p = \phi - \alpha, \text{ [}^\circ\text{]} \quad (12)$$

where \$\alpha\$ is the angle of attack of the airfoil.

The chord distribution is computed using Eq. (13), as follows:

$$c = \frac{8\pi r}{B \cdot C_l} (1 - \cos\phi), \text{ [m]} \quad (13)$$

where \$B\$ is the number of blades and \$C_l\$ is the lift coefficient of the airfoil.

The local solidity (\$s'\$) represents the fraction of the annular area occupied by the blades and is determined using the next equation:

$$s' = \frac{B \cdot c}{2\pi r}, \text{ [-]} \quad (14)$$

The loss factor \$F\$ indicates the mechanical power decrease at the blade tip, and is computed by the following expression:

$$F = \left(\frac{2}{\pi}\right) \cos^{-1} \left[e^{-\frac{(B)[R-r]}{(2r \sin\phi)}} \right], \text{ [-]} \quad (15)$$

The Glauert empirical relationship allows to compute the axial induction factor when the trust coefficient \$C_T\$ (Eq. 16) is greater than 0.96, using Eq. (17)

$$C_T = \frac{s'(1-a)^2(C_l \cos\phi + C_d \sin\phi)}{\sin^2\phi}, \text{ [-]} \quad (16)$$

where \$C_d\$ is the drag coefficient of the airfoil.

$$C_T = \frac{s'(1-a)^2(C_l \cos\phi + C_d \sin\phi)}{\sin^2\phi}, \text{ [-]} \quad (17)$$

The power coefficient \$C_P\$ indicates the fraction of wind power extracted by the rotor. To determine the design \$C_P\$ Eq. (18) is used.

$$C_P = \left(\frac{8}{\lambda N}\right) \sum_{i=k}^N F \sin^2\phi_i (\cos\phi_i - \lambda_r \sin\phi_i) (\sin\phi_i + \lambda_r \cos\phi_i) \left[1 - \left(\frac{C_d}{C_l}\right) \cot\phi_i\right] \lambda_r^2 d\lambda_r, \text{ [-]} \quad (18)$$

where \$N\$ is the number of elements that divide the blade and \$i\$ is the subscript that shows which blade element is being evaluated.

According to the Betz limit, the maximum value of \$C_P\$ that can be obtained is 0.5926, using an axial induction factor of 1/3 (Manwell et al., 2009). It means that the turbine can extract up to 59% of the energy contained in the wind.

2.4. Power coefficient calculation

Figure 3 shows the methodology behind BEM theory that is applied in the calculation of the power coefficient. This methodology requires as inputs: Number of blades (\$B\$), rotor radius (\$R\$), TSR, the lift and drag coefficients (\$C_l\$, \$C_d\$), and the angle of attack (\$\alpha\$) (Manwell et al., 2009).

Sections 2.4.1. and 2.4.2. show procedures to define the rotor geometry and to evaluate the power coefficient in terms of wind velocity. These results are used to build the power curve.

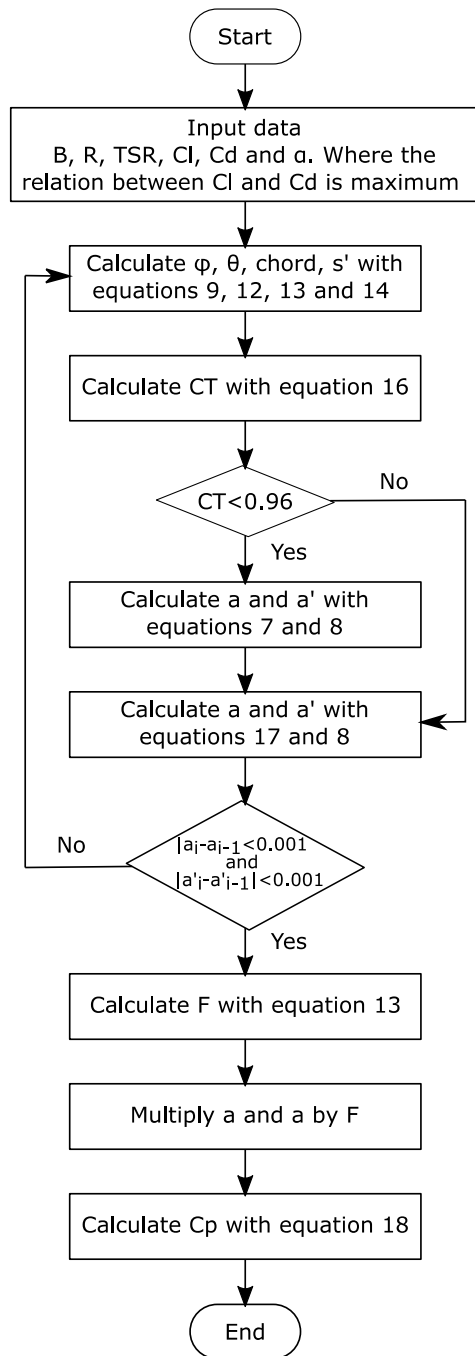


Figure 3: Flowchart of BEM theory.

2.4.1. Variation of the power coefficient in terms of TSR

Table 1 shows the initial data required to compute the power coefficient in terms of TSR for different rotor radius. The following airfoils are used: NACA 4415, 4418, 4421, 4424, 4430 and 4436 (Fuglsang et al., 2004; Khaled et al., 2017; Mamadaminov, 2013; Manwell et al., 2009). These are located in the blade according to defined considerations used by (Mohammadi et al., 2016) and (Adaramola, 2014). Using the XFOIL software the lift and drag coefficients are evaluated (Manwell et al., 2009; Massachusetts Institute of Technology, 2013). The value

of each coefficient is determined when the ratio between C_l and C_d is a maximum (Manwell et al., 2009).

Table 1. Identified points in the case study

Parameter	Value
R	35 – 60 [m]
TSR	4 – 10
N	10
Cl	
Cd	NACA 4 digits
α	

XFOIL requires as an input the Reynolds R number. This dimensionless number relate inertial forces over viscous forces, as it appears in the Eq. (19) (Dehouck et al., 2018; Takeyeldein et al., 2019):

$$R = \frac{\rho U c}{\mu} [-] \tag{19}$$

where ρ represents the air density [kg/m³], and μ represents the air viscosity [kg/m*s]. U is the wind velocity [m/s], and c is the chord of the airfoil [m]. The air density is compute by using Eq. (20).

$$\rho = 1,225 * \left(\frac{288}{t+273}\right) * e^{\left(\frac{-h}{8435}\right)}, [\text{kg/m}^3] \tag{20}$$

where h is the total height corresponding to the sum of all the height values in meters: Site (2720 m) and turbine, and t is the mean temperature of the site in °C (Cochancela & Astudillo, 2012).

The maximum power coefficient is chosen to define the rotor geometry.

2.4.2. Variation of the power coefficient in terms of the wind velocity

Table 2 shows the characteristics of the 1.5 MW Goldwind turbines that are used in the Villonaco wind power plant (Goldwind, 2015). The boot, nominal and stop velocities are used to build the power curve.

Table 2: Characteristics of the 1.5 MW Goldwind turbine.

Parameter	Value
B	3
R	35 [m]
Tower height	65 [m]
Boot velocity	3 [m/s]
Nominal velocity	12 [m/s]
Stop velocity	25 [m/s]

For the sake of the study, the turbine is assumed to be a variable velocity type (Manwell et al., 2009). In this kind of technology the rotation velocity increases and the TSR remains constant and equal to the optimal value between

the boot and rated velocities indicated in the power curve. While for the case of wind velocity greater than the rated, the TSR decreases and the rotation velocity remains constant and equal to the value determined for the case of the rated velocity to avoid damage (Jamieson, 2018; Lanzafame & Messina, 2010).

Using Eq. (11) the rotation velocity and the TSR are computed according to the wind velocity.

$$\Omega = \frac{\lambda U}{R}, [\text{rad/s}]$$

The power coefficient is evaluated between boot and stop velocities that are shown in Table 2.

2.5. Electric Power

The power curve of the turbine is determined by using the Eq. (21) (Letcher, 2017):

$$P_{electric} = \frac{1}{2} \pi * \rho * C_p * R^2 * U^3 * \eta_{mec} * \eta_{eléc}, [\text{W}] \quad (21)$$

It is assumed that both, the mechanical and electrical efficiencies (η_{mec} , $\eta_{eléc}$) are 0.9 (Hansen, 2008).

By using the power curve the real electric power can be computed along a period of one year following the process showed in the Figure 4 (Mathew & Philip, 2011). For this, the power $P(U)$ of the power curve and the probability $f(U)$, divided into intervals of 1.0 m/s, obtained from the probabilistic density function are multiplied (Ministerio de Electricidad y Energía Renovable, 2013).

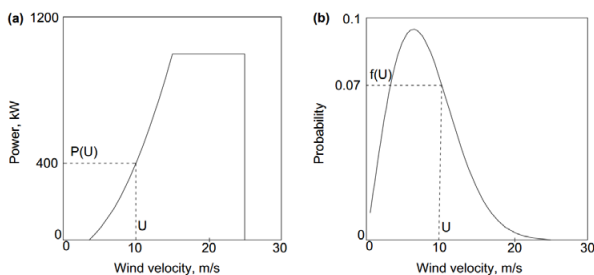


Figure 4: Integration of the power curves (a) and probability (b) to determine the energy produced (Mathew & Philip, 2011).

2.6. Relationship between rated power, height and diameter of the turbine

Expression (Manwell et al., 2009) indicated the rated power, which is defined by the nominal velocity increases as the height and the rotor diameter increases as well. Further, it is known that the tower height and the rotor diameter are two fundamental factors in the wind turbine design because they both have an impact on the cost of energy production (Lee et al., 2019). Thus, the influence on the energy production of the following variables are evaluated: tower height, nominal velocity and rotor radius. Table 3 shows the parameters considered in this analysis, the values are used commonly in modern turbines.

Table 3: Parameter variation.

Parameters			
Variation	Height [m]	Nominal velocity [m/s]	Radius [m]
1	65 – 140	15	35
2	65	10 – 15	35
3	140	15	35 – 60

2.7. Energy generated

The capacity factor FC is an indicator of the energy extraction efficiency, and it relates the energy generated E_{actual} and the maximum energy E_{ideal} that can be produced in ideal conditions. A period of time T is considered and computed using Eq. (22), according to (Letcher, 2017; Ministerio de Electricidad y Energía Renovable, 2013; Topaloğlu & Pehlivan, 2018).

$$FC = \frac{E_{actual}}{E_{ideal}} = \frac{T * P}{T * P_R} = \frac{P}{P_R}, [-] \quad (22)$$

where P is the power generated and P_R is the rated power of the turbine [W].

The annual energy generation is obtained by the multiplication of the rated power P_R , the number of hours during the year and the capacity factor FC as it is shown in the Eq. (23) (Letcher, 2017; Ministerio de Electricidad y Energía Renovable, 2013).

$$E = 8760 * P_R * FC, [\text{W}] \quad (23)$$

3. Results and Discussion

Due to the lack of a significant variation of the wind velocity in terms of height, the data of the wind velocity from the 62.8 m was used in the statistical analysis because this value is close enough to the height of the CEV turbines.

The shape and scale Weibull factors, the most probable velocity and the velocity that produce more energy are shown in Table 4. The most probable velocity has a value equal to 10.50 m/s and the velocity that produce more energy is equal to 12.46 m/s. This last value is close to the nominal velocity considered in this study, whereby the most suitable velocity in the design process must be closer to 12.46 m/s based on the criteria defined by (Oyedepo et al., 2012).

Table 4: Shape and scale Weibull factors.

Factor	Value
k	4.02 [-]
c	11.27 [m/s]
U_{mp}	10.50 [m/s]
$U_{máxE}$	12.46 [m/s]

The shape and scale factors from Table 4 are similar to the ones obtained in the study called “Analysis of the behavior of the wind power plant in extreme conditions”, which was done in the year 2014 by the Ecuadorian National Institute of Energy Efficiency and Renewable Energies (INER). In this study the Weibull shape and scale factors are equal to 2.07 and 11.58 m/s, respectively for the measurements of the wind velocities in Villonaco wind power plant, between 2012 and 2014 at a height equal to 60 m (Instituto Nacional de Eficiencia Energética y Energías Renovables, 2014).

Figure 5a shows the average probability of the wind velocity divided into 1.0 m/s intervals.

In the analysis of the temperature measurements in the CEV, the monthly mean temperature in the site is 11°C.

Figure 5b shows the Reynolds number in terms of a dimensionless radius according to the size of the rotor. The dimensionless radius relates the position of each one of the N elements (measured from the rotation axis of the turbine) with the rotor radius. To obtain this dimensionless parameter it is assumed a viscosity of the air equal to 1.81×10^{-5} (Viscosidad Del Aire, 2012). This parameter has a maximum value when the radius is equal to 60 m, while it is minimum when the radius is equal to 35 m. These results are among the established range between 1×10^6 and 9×10^6 for the case of wind turbines (Ge et al., 2015).

Figures 5c and 5d show the distribution of the lift and drag coefficients along the Blade. The angle of attack, when the ratio stays between C_l and C_d , takes a maximum value equal to 7° for all the airfoils selected. The results agreed

with previous studies carried on by Burton et al. (Burton et al., 2001), where it shows that for a wind turbine with a TSR equal to 8, the angle of attack remains approximately constant.

Figure 5c shows a maximum value of the lift coefficient for the specific radius equal to 60, while a minimum value is found when the radius equal to 35 m is used. It is evident an increase tendency along the Blade for this coefficient as its shown by (Mamadaminov, 2013).

Figure 5d shows a maximum value of the drag coefficient for the case where the radius is equal to 35 m, and a minimum value for the case where the radius is equal to 60 m. In addition, it is observed that this coefficient is maximum at the root and decreases until it remains approximately constant from 30% of the length of the blade. These results agree with the values used in (Mamadaminov, 2013).

The chord distribution along the Blade for each rotor radius (Figure 6a) shows that the chord values are minimum when the radius is equal to 35 m and maximum when the radius is equal to 60 m. These results have a similar tendency with respect to the results obtained for a turbine which runs at a TSR condition equal to 7, as exposed by (Manwell et al., 2009).

The power coefficient in terms of TSR and the rotor radius is shown in Figure 6b. The maximum value of the coefficient is in between 0.467 and 0.473 when the TSR value is equal to 8.

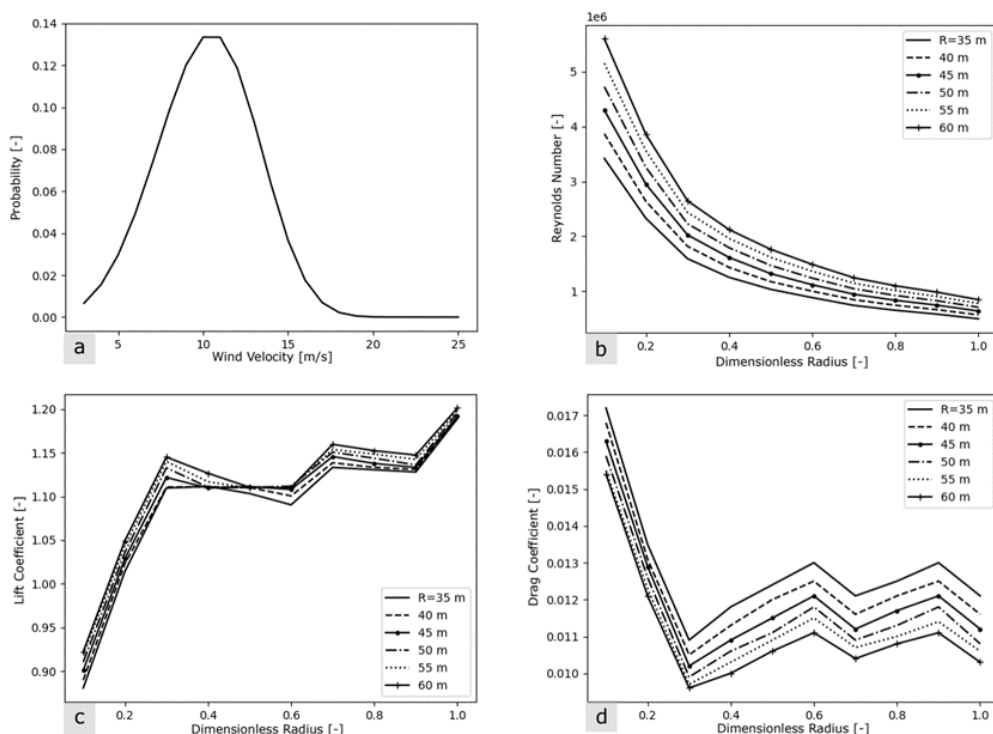


Figure 5: (a) Probabilistic distribution; (b) Reynolds number; (c) Lift coefficients; (d) Drag coefficients.

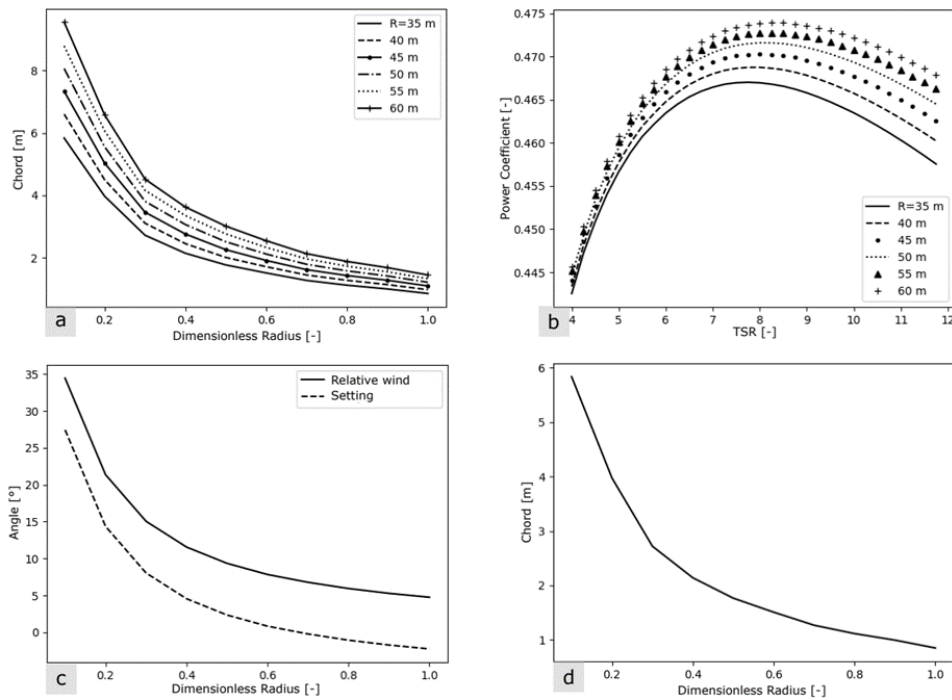


Figure 6: (a) Chord distribution in terms of rotor radius; (b) Power coefficient in terms of TSR; (c) Relative wind angle and setting angle; (d) Chord distribution.

These results are within the established range for modern wind turbines as expressed in studies carried out by (Letcher, 2017) and (Ge et al., 2015).

Since the variation of the power coefficient is not significant, the radius of 35 m and a TSR equal to 8 are selected to define the geometry of the turbine rotor.

Figure 6c shows the variation of the relative wind angle and the setting angle in terms of the dimensionless radius. Both angles show a decrease tendency, having greater values when they are closer to the center of rotation.

In Figure 6d it is pointed out the value of the chord that is equal to 5.8 m at the root and 0.85 m at the tip. These

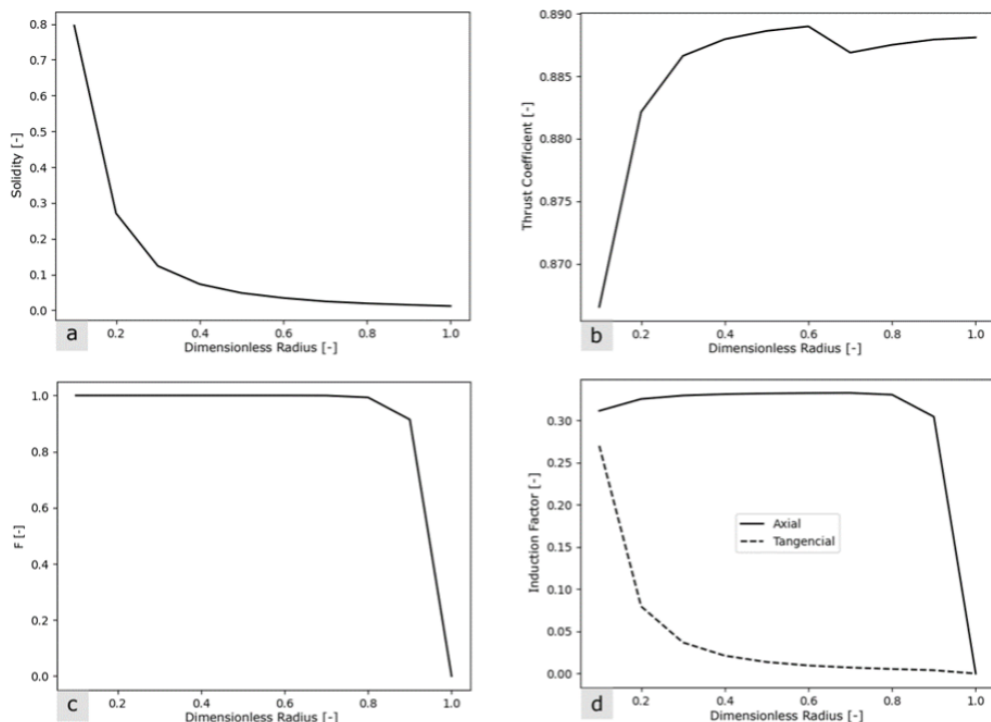


Figure 7: (a) Local solidity; (b) Thrust coefficient; (c) Blade tip loss factor; (d) Axial and tangential induction factors.

results have a similar tendency to that obtained for a turbine that operates at TSR equal to 7 as stated by Manwell et al. (Manwell et al., 2009).

Figure 7a shows the variation of the solidity in terms of the dimensionless radius, where it is evident a decreasing tendency of this factor having values of 0.79 at the root and 0.012 at the tip. In the study by Dereje et al. (Dereje & Sirahbizu, 2019), the solidity takes a value of 0.018 at the tip of the blade of a 36 m radius rotor.

Thrust coefficient along the blade (Figure 7b) takes a value equal to 0.86 at the root and 0.88 for the tip and middle zones. These values show that the turbine is working as a windmill as it is stated by (Manwell et al., 2009).

The F factor in terms of the dimensionless radius (Figure 7c) is equal to 1 until the blade length is equivalent to 70%, while in the last 30% it takes values of 0.99, 0.91 and 0. These results are in correspondence with the findings in the study carried out by Burton et al. (Burton et al., 2001).

Figure 7d shows the axial and tangential induction factors variation in terms of the dimensionless radius. The first factor is equal to 0.33 in 90% of the blade and in the final 10% it is equal to 0; while the second factor is equal to 0.27 at the root and 0 at the tip. The values of the axial and tangential induction factors, which have a similar tendency with the results obtained for a turbine with a TSR of 7.5 as described by (Manwell et al., 2009).

Figure 8a shows when the wind velocity is between 3 and 12 m/s, the rotation velocity increases from 0.68 rad/s to 2.74 rad/s, and the power coefficient remains constant with a value equal to 0.11. In addition, there is a region delimited by the most probable wind velocity, and the velocity which carries the most energy. Both velocities obtained by the statistical analysis.

The rotation velocity and the calculated power coefficient correspond to that obtained for a variable velocity turbine according to the studies carried out by Lanzafame & Messina (2010) and Saint-Drenan et al. (2019).

The power curve calculated for a turbine with the same dimensions (rotor radius and height) as those of the turbines used in the CEV is indicated in Figure 8b. The rated power obtained is 1.25 MW.

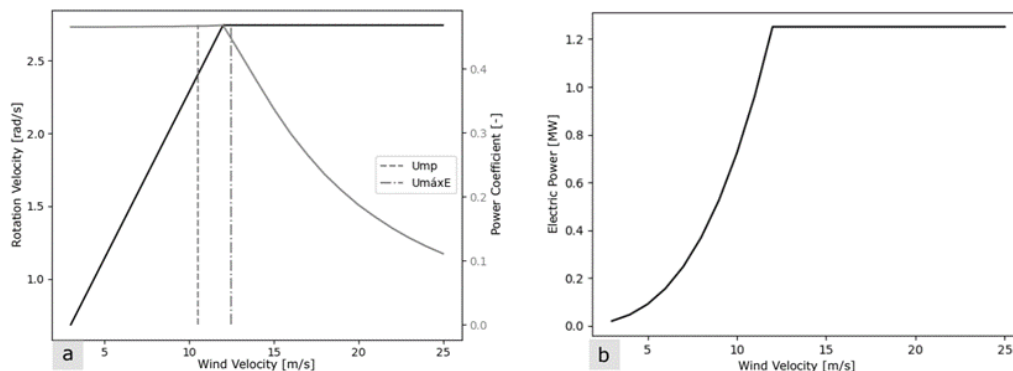


Figure 8: (a) Rotation velocity and power coefficient in terms of wind velocity; (b) Power curve calculated.

Table 5: Real energy produced and Real capacity factor.

Year	Energy [GWh]	Capacity Factor [-]
2014	6.79	0.52
2015	8.40	0.63
2016	6.97	0.53
2017	6.10	0.46
2018	5.59	0.50
Average	6.77	0.53

Table 6: Comparison between real values and calculated values of energy and capacity factor.

Parameter	Real	Calculated	Relative error [%]
Energy [GWh]	6.77	6.80	0.44
Capacity Factor [-]	0.53	0.62	14.09

Using the power curve illustrated in Figure 8b and the probability density function in Figure 5a, it is determined that the energy produced, and the capacity factor are equal to 6.80 GWh and 0.62, respectively.

The data of energy produced and the average capacity factor for the CEV turbine (Table 5), were obtained from the Accountability reports that CELEC EP GENSUR carried out annually (Corporación Eléctrica del Ecuador, 2015, 2016b, 2017, 2018, 2019a).

The comparison between the real and calculated energy and capacity factor values are shown in Table 6. The calculated results are greater than the real ones, having an error of 0.44% in the energy and 14.09% for the energy factor capacity.

The margin of error is within the allowed limit, taking into consideration the criteria developed by Hidalgo et al. (2015), where it was stated that an acceptable prediction can have a relative error less than 20%.

The variation of air density according to the height of the turbine is shown in Figure 9a. The density decreases as the height increases, at 2785 m is equal to 0.893 kg/m³

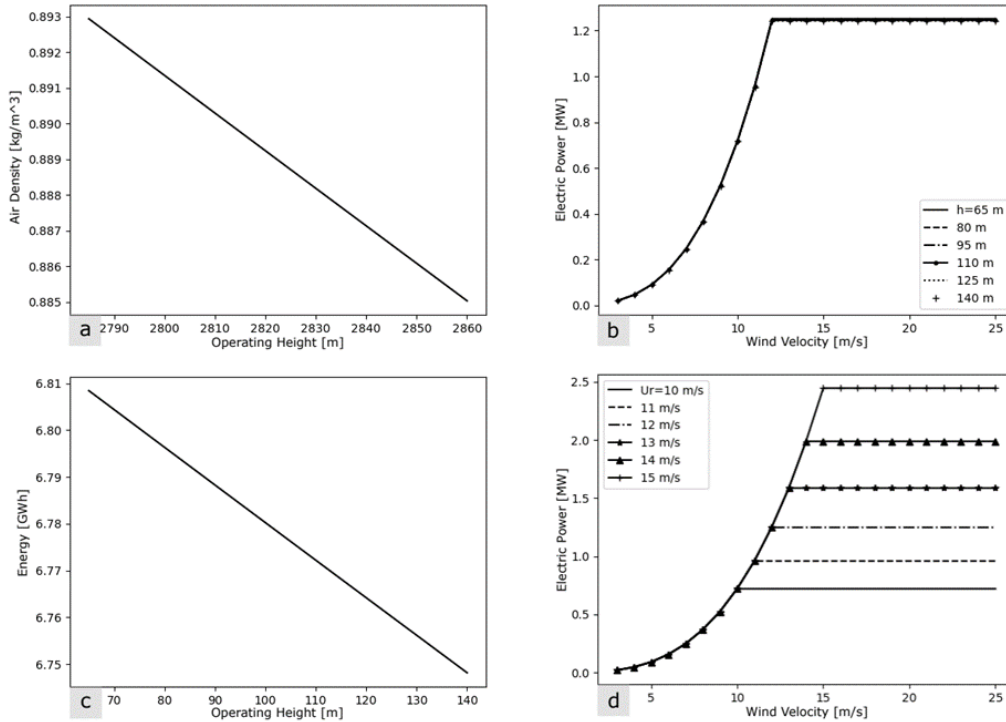


Figure 9: (a) Air density in terms of height; (b) Electric Power against height; (c) Energy produced in terms of height; (d) Power in terms of nominal velocity.

while at 2860 m it takes a value of 0.885 kg/m^3 , having a difference of 0.89%.

The effect of the variation of the height in the electric power is shown in Figure 9b. It is evident that the change is not significant, therefore it is assumed that within this range of height the density remains constant.

The capacity factor is equal to 0.62 and remains unchanged with the change in height. Figure 9c indicates the energy produced as a function of the height of the turbine, and it is observed that for a height of 65 m, 6.80 GWh is generated, while for a height of 140 m, 6.74 GWh is produced, representing a decrease in energy produced by 0.88%. These results agree with those obtained when

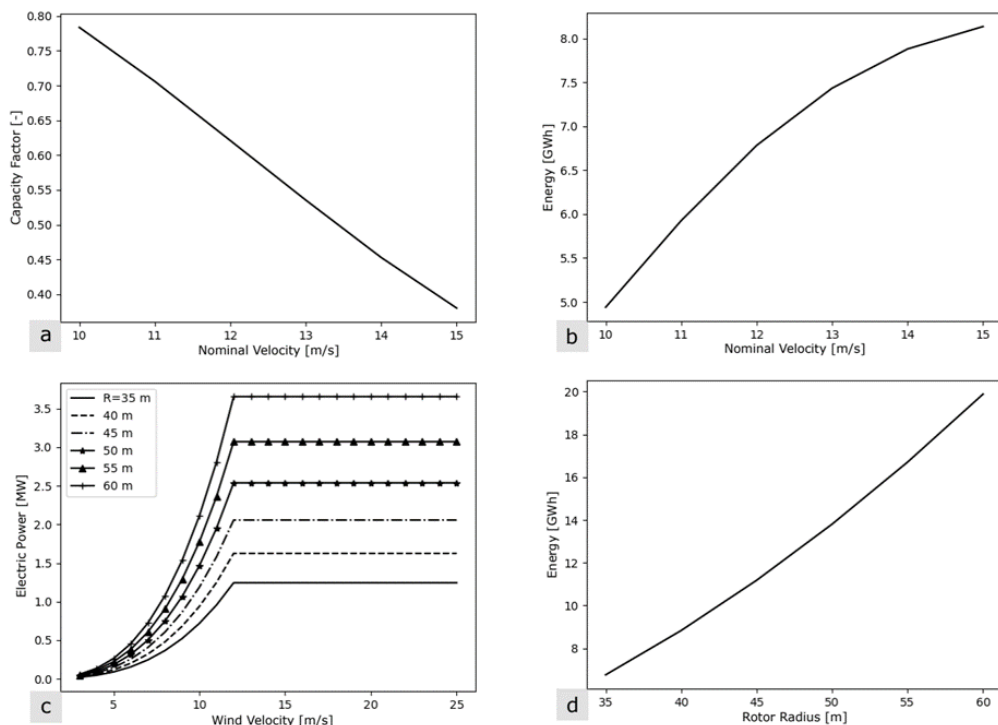


Figure 10: (a) Capacity factor variation; (b) Energy produced in terms of nominal velocity; (c) Power in terms of rotor radius; (d) Energy produced according to the rotor radius.

comparing the energy produced by turbines with a height difference of 25 m according to the study carried out by (Gul et al., 2019).

The effect of the variation of the nominal velocity on the electrical power is illustrated in Figure 9d. The rated power is equal to 0.71 MW at a nominal velocity of 10 m/s and reaches a value of 2.44 MW at 15 m/s. This expresses an increase of 243.66%.

The variation of the capacity factor as a function of the nominal velocity is shown in Figure 10a. It shows that this factor decreases with the increase in the nominal velocity, being equal to 0.78 at 10 m/s and 0.38 at 15 m/s, which represents a reduction of 51.49%.

Figure 10b shows the energy production as a function of the nominal velocity, it is observed that at a velocity of 10 m/s 4.93 GWh is generated and for a velocity of 15 m/s 8.13 GWh is produced, this shows an increase of 64.90%. This tendency is similar to that evidenced when the energy generated by turbines that differ by 0.5 m/s in their nominal velocity was compared in the study carried out by (Mahmood et al., 2019).

The effect of the variation of the rotor radius on the electric power generated is indicated in Figure 10c. The variation of the power coefficient as a function of the wind velocity is the same for each evaluated rotor radius because this coefficient does not present a substantial change as described in Figure 6b. The nominal power for the radius equal to 35 m is 1.24 MW and the corresponding one for 60 m is 3.65 MW, which corresponds to an increase of 194.35%.

The capacity factor is equal to 0.62 and remains constant with respect to the radius variation. Energy production as a function of the rotor radius (Figure 10d), shows that 6.76 GWh is generated for the radius equal to 35 m, while for the 60 m radius, 19.87 GWh is produced, expressing an increase of 193.93%. This tendency is similar to that obtained when the energy generated by turbines with different rotor sizes was compared in the study of (Gul et al., 2019).

References

- Adaramola, M. (2014). *Wind turbine technology: Principles and design*. Apple Academic Press, Inc. [https://doi.org/10.1016/s0038-092x\(97\)82047-6](https://doi.org/10.1016/s0038-092x(97)82047-6)
- Arconel. (2015). *Ecuador posee un 51,78% de energía renovable*. <https://www.regulacionelectrica.gob.ec/ecuador-posee-un-5155-de-energia-renovable/%0A>
- Bakirci, M., & Yilmaz, S. (2018). Theoretical and computational investigations of the optimal tip-speed ratio of horizontal-axis wind turbines. *Engineering Science and Technology, an International Journal*, 21(6), 1128–1142. <https://doi.org/10.1016/j.jestch.2018.05.006>
- Biadgo, A.M., & Aynekulu, G. (2017). Aerodynamic design of horizontal axis wind turbine blades. *FME Transactions*, 45(4), 647–660. <https://doi.org/10.5937/fmet1704647M>
- Burton, T., Sharpe, D., Jenkins, N., & Bossanyi, E. (2001). *Wind Energy Handbook*. In *Wind Energy Handbook* (First edit). Wiley. <https://doi.org/10.1002/9781119992714.ch9>
- Carta González, J.A., Calero Pérez, R., Colmenar Santos, A., & Castro Gil, M.A. (2009). *Centrales de energías renovables: Generación eléctrica con energías renovables*. Pearson Educación S.A.

4. Conclusions

In the present study, a programming code was developed using Python, in which Numpy and Matplotlib libraries are used to analyze the parameters that maximize the annual energy production of a wind turbine.

A methodology was developed to define the geometric characteristics of a wind turbine and compute the annual energy generated using the wind velocity measurements recorded during the years 2015 and 2019 in the CEV. By means of the statistical analysis of the wind velocities, it is determined that the mean factors of the Weibull shape, scale and the velocities: most probable and the one that carries the greatest energy are equal to 4.02, 11.07 m/s, 10, 50 m/s and 12.46 m/s, respectively. It was determined that the power coefficient as a function of TSR does not represent a significant change when varying the rotor radius, obtaining an average value of 0.47, which is within the range established in current technology according to Letcher.

The reliability of the programming code was verified by obtaining a relative error less than 20% for the difference between real and calculated values of energy produced and capacity factor as it is defined by (Hidalgo et al., 2015). It was observed that the increase in the nominal velocity from 10 m/s to 15 m/s produces a reduction of 51.49% of the capacity factor, while for the variations in height and rotor radius, the value of this factor is maintained in 0.62.

Finally, the increase in the rotor radius and the nominal velocity produce an increase of 193.93% and 64.90% of the energy generated, respectively; and on the other hand, increasing the height of the turbine causes a reduction of 0.88% in the energy produced.

Acknowledgments

The authors gratefully acknowledge the financial support provided by Escuela Politécnica Nacional for the development of the project PII-DIM-2019-06

Parametric study of a horizontal axis wind turbine with similar characteristics to those of the Villonaco wind power plant

- Cochancela, J., & Astudillo, P. (2012). *Análisis energético de centrales eólicas*. In Universidad de Cuenca. <http://dspace.ucuenca.edu.ec/jspui/bitstream/123456789/5022/1/Tesis.pdf>
- Corporación Eléctrica del Ecuador. (2015). *Informe de rendición de cuentas 2014 Unidad de Negocio GEN-SUR*. <https://www.celec.gob.ec/gensur/index.php>
- Corporación Eléctrica del Ecuador. (2016a). *Central Eólica Villonaco genera el 152% de lo planificado CE-LEC EP-GENSUR*. <https://www.celec.gob.ec/gensur/index.php/67-central-eolica-villonaco-genera-el-152-de-lo-planificado>
- Corporación Eléctrica del Ecuador. (2016b). *Informe de rendición de cuentas 2015 Unidad de Negocio GENSUR*. <https://www.celec.gob.ec/gensur/index.php>
- Corporación Eléctrica del Ecuador. (2017). *Informe de Rendición de Cuentas 2016 Unidad de Negocio GENSUR*. <https://www.celec.gob.ec/gensur/index.php>
- Corporación Eléctrica del Ecuador. (2018). *Informe de rendición de cuentas 2017 Unidad de Negocio GENSUR*. <https://www.celec.gob.ec/gensur/index.php>
- Corporación Eléctrica del Ecuador. (2019a). *Informe de rendición de cuentas 2018 Unidad de Negocio GENSUR*. <https://www.celec.gob.ec/gensur/index.php>
- Corporación Eléctrica del Ecuador. (2019b). *Producción anual de la Central Eólica Villonaco*. <https://www.celec.gob.ec/gensur/index.php/cev/central-eolica-villonaco-en-cifras>
- Dehouck, V., Lateb, M., Sacheau, J., & Fellouah, H. (2018). Application of the BEM Theory to Design HAWT Blades. *Journal of Solar Energy Engineering, Transactions of the ASME*, 140(1), 014501. <https://doi.org/10.1115/1.4038046>
- Dereje, G., & Sirahbizu, B. (2019). Design and Analysis of 2MW Horizontal Axis Wind Turbine Blade. *International Journal of Innovative Science, Engineering & Technology*, 6(5).
- El Khchine, Y., & Sriti, M. (2018). Improved blade element momentum theory (BEM) for predicting the aerodynamic performances of horizontal axis wind turbine blade (HAWT). *Technische Mechanik*, 38(2), 191–202. <https://doi.org/10.24352/UB.OVGU-2018-028>
- Fuglsang, P., Bak, C., Gaunaa, M., & Antoniou, I. (2004). Design and verification of the Risø-B1 airfoil family for wind turbines. *Journal of Solar Energy Engineering, Transactions of the ASME*, 126(4), 1002–1010. <https://doi.org/10.1115/1.1766024>
- Ge, M., Fang, L., & Tian, D. (2015). Influence of reynolds number on multi-objective aerodynamic design of a wind turbine blade. *PLoS ONE*, 10(11), 1–25. <https://doi.org/10.1371/journal.pone.0141848>
- Goldwind. (2015). Goldwind 1.5MW. <https://www.goldwindamericas.com/15-mw-pmdd>
- Gul, M., Tai, N., Huang, W., Nadeem, M.H., & Yu, M. (2019). Assessment of wind power potential and economic analysis at Hyderabad in Pakistan: Powering to local communities using wind power. *Sustainability*, 11(5), 1391. <https://doi.org/10.3390/su11051391>
- Hansen, M.O.L. (2008). *Aerodynamics of Wind Turbines* (Second ed, Vol. 53, Issue 9). Earthscan.
- Hidalgo, V., Luo, X.W., Escaler, X., Ji, B., & Aguinaga, A. (2015). Implicit large eddy simulation of unsteady cloud cavitation around a plane-convex hydrofoil. *Journal of Hydrodynamics*, 27(6), 815–823. [https://doi.org/10.1016/S1001-6058\(15\)60544-3](https://doi.org/10.1016/S1001-6058(15)60544-3)
- Instituto Nacional de Eficiencia Energética y Energías Renovables. (2014). *Análisis del comportamiento de un parque eólico en condiciones extremas*.
- International Energy Agency. (2019). *Renewables – World Energy Outlook 2019*. <https://www.iea.org/reports/world-energy-outlook-2019/renewables#abstract>
- Jamieson, P. (2018). *Innovation in Wind Turbine Design* (Second ed.). Wiley. <https://doi.org/10.1002/9781119137924>
- Khaled, M., Mohamed Ibrahim, M., ElSayed Abdel Hamed, H., & Abdel Gawad, A.F. (2017). Aerodynamic Design and Blade Angle Analysis of a Small Horizontal–Axis Wind Turbine. *American Journal of Modern Energy*, 3(2), 23–27. <https://doi.org/10.11648/j.ajme.20170302.12>
- Lanzafame, R., & Messina, M. (2010). Horizontal axis wind turbine working at maximum power coefficient continuously. *Renewable Energy*, 35(1), 301–306. <https://doi.org/10.1016/j.renene.2009.06.020>
- Lee, J.T., Kim, H.G., Kang, Y.H., & Kim, J.Y. (2019). Determining the optimized hub height of wind turbine using the wind resource map of South Korea. *Energies*, 12(15), 2949. <https://doi.org/10.3390/en12152949>

- Letcher, T.M. (2017). *Wind Energy Engineering: A Handbook for Onshore and Offshore Wind Turbines*. Elsevier. <https://doi.org/10.1016/B978-0-12-809451-8.00001-1>
- Mahmood, F.H., Resen, A.K., & Khamees, A.B. (2019). Wind characteristic analysis based on Weibull distribution of Al-Salman site, Iraq. *Energy Reports*, 6(September), 79–87. <https://doi.org/10.1016/j.egy.2019.10.021>
- Mamadaminov, U.M. (2013). *Review of Airfoil Structure for Wind Turbine Blades*. Department of Electrical Engineering and Renewable Energy REE, 515., September 2013, 1–8.
- Manwell, J.F., McGowan, J.G., & Rogers, A.L. (2009). *Wind energy explained: theory, design and application* (Second ed.). John Wiley & Sons. <https://doi.org/10.1002/9781119994367>
- Massachusetts Institute of Technology. (2013). *Xfoil*. <https://web.mit.edu/drela/Public/web/xfoil/>
- Mathew, S., & Philip, G.S. (2011). *Advances in Wind Energy Conversion Technology*. Springer. <https://doi.org/10.1007/978-3-540-88258-9>
- Ministerio de Electricidad y Energía Renovable. (2013). *Atlas Eólico del Ecuador con fines de generación eléctrica*.
- Mohammadi, M., Mohammadi, A., & Farahat, S. (2016). A new method for horizontal axis wind turbine (HAWT) blade optimization. *International Journal of Renewable Energy Development*, 5(1), 1–8. <https://doi.org/10.14710/ijred.5.1.1-8>
- Najafian Ashrafi, Z., Ghaderi, M., & Sedaghat, A. (2015). Parametric study on off-design aerodynamic performance of a horizontal axis wind turbine blade and proposed pitch control. *Energy Conversion and Management*, 93, 349–356. <https://doi.org/10.1016/j.enconman.2015.01.048>
- Oyedepo, S.O., Adaramola, M.S., & Paul, S.S. (2012). Analysis of wind speed data and wind energy potential in three selected locations in South-East Nigeria. *International Journal of Energy and Environmental Engineering*, 3(1), 1–11. <https://doi.org/10.1186/2251-6832-3-7>
- Rehman, S., Alam, M.M., Alhems, L.M., & Rafique, M.M. (2018). Horizontal Axis Wind Turbine Blade Design Methodologies for Efficiency Enhancement-A Review. *Energies*, 11(3). <https://doi.org/10.3390/en11030506>
- Renewable Energy World. (2019). *Wind Power Technology*. <https://www.renewableenergyworld.com/types-of-renewable-energy/wind-power-tech/#gref>
- Ritchie, H., & Roser, M. (2017). *Renewable Energy. Our World in Data*. <https://ourworldindata.org/renewable-energy>
- Saint-Drenan, Y.M., Besseau, R., Jansen, M., Staffell, I., Troccoli, A., Dubus, L., Schmidt, J., Gruber, K., Simões, S.G., & Heier, S. (2019). A parametric model for wind turbine power curves incorporating environmental conditions. *Renewable Energy*, 157, 754–768. <https://doi.org/10.1016/j.renene.2020.04.123>
- Takeyeldein, M.M., Lazim, T.M., Nik Mohd, N.A.R., Ishak, I.S., & Ali, E.A. (2019). Wind turbine design using thin airfoil SD2030. *Evergreen Joint Journal of Novel Carbon Resource Sciences & Green Asia Strategy*, 6(2), 114–123. <https://doi.org/10.5109/2321003>
- Topaloğlu, F., & Pehlivan, H. (2018). Analysis of Wind Data, Calculation of Energy Yield Potential, and Micrositing Application with WASP. *Advances in Meteorology*, 2018. <https://doi.org/10.1155/2018/2716868>
- Viscosidad del aire. (2012). <https://didactica.fisica.uson.mx/tablas/viscosidad.htm>